

# 1 Morphologic and Morphometric Differences between Gullies Formed 2 in Different Substrates on Mars: New Insights into the Gully 3 Formation Processes

4 Rishitosh K. Sinha<sup>1,2</sup>, Dwijesh Ray<sup>1</sup>, Tjalling De Haas<sup>3</sup>, Susan J. Conway<sup>4</sup>, Axel Noblet<sup>4</sup>

5 <sup>1</sup> Physical Research Laboratory, Ahmedabad 380009, Gujarat, India

6 <sup>2</sup> Indian Institute of Technology, Gandhinagar 382355, Gujarat, India

7 <sup>3</sup> Faculty of Geoscience, Universiteit Utrecht, Princetonlaan 8a, 3584 CB Utrecht, the Netherlands

8 <sup>4</sup> Nantes Université, Université d'Angers, Le Mans Université, CNRS UMR 6112 Laboratoire de Planétologie et Géosciences,  
9 France

10

11 *Correspondence to:* Rishitosh K. Sinha (rishitosh@prl.res.in)

12 **Abstract.** Martian gullies are kilometer-scale geologically young features with a source alcove, transportation channel, and  
13 depositional fan. On the walls of impact craters, these gullies typically incise into bedrock or surfaces modified by latitude  
14 dependent mantle (LDM; inferred as consisting of ice and admixed dust) and glaciation. To better understand the differences  
15 in the alcoves and fans of gullies formed in different substrates and infer the flow types that led to their formation, we have  
16 analyzed the morphology and morphometry of 167 gully systems in 29 craters distributed between 30°S and 75°S. Specifically  
17 we measured length, width, gradient, area, relief, and relief ratio of the gully alcoves and fans, Melton ratio, relative concavity  
18 index, and perimeter, form factor, elongation ratio and circularity ratio of the gully alcoves. Our study reveals that gully alcoves  
19 formed in LDM/glacial deposits are more elongated than the gully alcoves formed in bedrock, and possess a distinctive V-  
20 shaped cross section. We have found that the mean gradient of fans formed by gullies sourced in bedrock is steeper than the  
21 mean gradient of fans of gullies sourced in LDM/glacial deposits. These differences between gullies were found to be  
22 statistically significant and discriminant analysis has confirmed that alcove perimeter, alcove relief and fan gradient are the  
23 most important variables for differentiating gullies according to their source substrates. The comparison between the Melton  
24 ratio, alcove length and fan gradient of Martian and terrestrial gullies reveals that Martian gully systems were likely formed  
25 by terrestrial debris-flow like processes. Present-day sublimation of CO<sub>2</sub> ice on Mars may have provided the adequate flow  
26 fluidization for the formation of deposits akin to terrestrial debris-flow like deposits.

## 27 1 Introduction

28 Gullies are found on steep slopes polewards of about 30° latitude in both hemispheres on Mars and manifest as kilometer-  
29 scale, geologically young features (formed within the last few million years) comprising an alcove, channel, and depositional  
30 fan (Malin and Edgett, 2000; Dickson et al., 2007; Reiss et al., 2004; Schon et al., 2009). Gullies occur in a wide assortment

31 of settings, varying from the walls and central peaks of craters to walls of valleys, and steep faces of dunes, hills and polar pits  
32 (e.g. Balme et al., 2006; Dickson et al., 2007; Dickson and Head, 2009; Conway et al., 2011, 2015; Harrison et al., 2015). On  
33 the walls of craters, gullies are found to have incised into (1) surfaces covered by latitude dependent mantle (LDM; e.g. Mustard  
34 et al., 2001; Dickson et al., 2012, 2015), (2) surfaces modified by former episodes of glaciation (Conway et al., 2018; de Haas  
35 2019a; Sinha and Vijayan, 2017), and (3) bedrock (e.g. Johnsson et al., 2014; de Haas et al., 2019a; Sinha et al., 2020). Detailed  
36 investigation of the gullies formed over these different substrates is key to understanding the intricacies of past processes by  
37 which these gullies have formed on Mars (Conway et al., 2015; de Haas et al., 2019a).

38 A variety of models have been proposed to explain the formation of gullies, which include: (1) dry flows triggered by  
39 sublimation of CO<sub>2</sub> frost (e.g. Cedillo-Flores et al., 2011; Dundas et al., 2012, 2015; Pilorget and Forget, 2016; de Haas et al.,  
40 2019b), (2) debris-flows of an aqueous nature (e.g. Costard et al., 2002; Levy et al., 2010; Conway et al., 2011; Johnsson et  
41 al., 2014; de Haas et al., 2019a; Sinha et al., 2020), and (3) fluvial flows (e.g. Heldmann and Mellon, 2004; Heldmann et al.,  
42 2005; Dickson et al., 2007; Reiss et al., 2011). To better understand the gully formation processes, morphometric investigation  
43 of gullies formed over different substrates needs to be undertaken at a level of detail previously not attempted.

44 The global distribution of gullies shows a spatial correlation with the landforms indicative of glaciation and LDM deposition  
45 on Mars (e.g. Levy et al., 2011; Dickson et al., 2015; Harrison et al., 2015; Conway et al., 2018; de Haas et al., 2019a; Sinha  
46 et al., 2020). With respect to glacial landforms, many gullies have formed into viscous flow features (VFFs) and they are found  
47 in the same latitude ranges between 30°-60° (e.g. Arfstrom and Hartmann, 2005; de Haas et al., 2019a). VFFs are defined as  
48 an umbrella term for glacial-type formations covering a broad range of landforms that include lobate debris aprons (LDAs),  
49 concentric crater fills (CCFs), and lineated valley fills (LVFs) (e.g. Squyres, 1978; Levy et al., 2009a; Baker et al., 2010;  
50 Hargitai, 2014). Together, they are inferred to be similar to terrestrial debris-covered glaciers (Plaut et al., 2009). With respect  
51 to LDM, gullies are mostly found on the pole-facing slopes of crater walls at lower mid-latitudes (30-45°) (e.g. Balme et al.  
52 2006; Kneissl et al. 2010; Harrison et al. 2015; Conway et al. 2017), wherein, LDM is found to be dissected (e.g. Mustard et  
53 al., 2001; Milliken et al., 2003; Head et al., 2003). In the higher latitudes (>45°), LDM is found to be continuous (e.g.  
54 Kreslavsky and Head, 2000), and gullies are evident at both the pole and equator facing slopes (e.g. Balme et al. 2006; Kneissl  
55 et al. 2010; Harrison et al. 2015; Conway et al. 2017). Gullies formed on the formerly glaciated walls of craters are fed from  
56 alcoves that do not extend up to the crater rim, and appear elongated to V-shaped, implying gully-channel incision into ice-  
57 rich, unlithified sediments (e.g. Aston et al., 2011; de Haas et al., 2019a). The alcoves, channels and fan deposits of gullies  
58 formed within craters covered by a smooth drape of LDM, are usually found to have experienced multiple episodes of LDM  
59 covering and subsequent reactivation of some of the pre-existing channels or formation of fresh channels within the draped  
60 LDM deposits (e.g. Dickson et al., 2015; de Haas et al., 2019a). Additionally, there are gullies that directly emanate from well-  
61 defined bedrock alcoves that cut into the crater rim in the absence of LDM and/or glacial deposits (e.g. Johnsson et al., 2014;  
62 de Haas et al., 2019a; Sinha et al., 2020). Gullies formed in these craters have alcoves with sharply defined crests and spurs,

63 exposing the underlying bedrock, and meter-sized boulders are found throughout the gully system (e.g. Johnsson et al., 2014;  
64 de Haas et al., 2019a; Sinha et al., 2020). Further, De Haas et al., 2015a found that the stratigraphy of the fans whose source  
65 area was in bedrock were more boulder-rich than those fans fed by catchments in LDM. The findings in these studies suggest  
66 that a more detailed investigation of the morphology and morphometry of the gullies formed over contrasting substrates is  
67 important for improving our understanding of the formative mechanisms of gullies.

68 In this work, we focus on addressing the following research questions:

69 (1) Do the morphologies and morphometries of gully systems formed in different substrates differ (i.e. LDM/glacial deposits  
70 and bedrock)?

71 (2) How do the morphometric characteristics of gullies formed on Mars compare to those formed by a range of processes on  
72 Earth, and what does that tell us about the formative processes of Martian gullies?

73 To parameterize the morphometry we will primarily study long profiles. Previously, only a few studies have analyzed the  
74 morphometric characteristics of the gullies by studying their long profiles (e.g. Yue et al., 2014; Conway et al., 2015; De Haas  
75 et al., 2015a; Hobbs et al., 2015). These studies have focused observations on a part of the gully system and suggested that the  
76 differences in the properties of substrate into which the gullies incise play a significant role in promoting the flows that led to  
77 gully formation. Hence, for a more detailed differentiation of the gully types and interpretation of the dominant flow type that  
78 led to gully formation on Mars, quantification of the morphometric characteristics of the entire gully system is crucial.

## 79 **2 Study sites and datasets**

80 We characterize the morphologies and morphometries of gullies in 29 craters distributed over the southern hemisphere of Mars  
81 between 30° S and 75° S latitude (Fig. 1). These 29 craters are selected based on the availability of publicly released High  
82 Resolution Imaging Science Experiment (HiRISE) stereo-pair based digital terrain models (DTMs) or the presence of suitable  
83 HiRISE stereo-pair images to produce a DTM ourselves. The HiRISE stereo-pair images are usually ~0.25 - 0.5 m/pixel  
84 (McEwen et al., 2007), so the DTM post spacing is ~1-2 m with vertical precision in the range of tens of centimeters (Kirk et  
85 al., 2008). Among the 29 gullied craters, publicly released DTMs are available for 25 craters  
86 (<https://www.uahirise.org/hiwish/maps/dtms.jsp> - last accessed 18th September 2021) (Table 1). For the remaining 4 craters,  
87 we produced DTMs with the software packages USGS ISIS and BAE Systems SocetSet (Table 1) (Kirk et al., 2008). We  
88 investigated HiRISE images of these 29 gullied craters for detailed morphological characterization of the substrate into which  
89 the crater wall gullies incise (Table 1).

90

91

92 **Table 1.** Summary of the craters included in this study, their locations, number of gullies investigated from the crater, substrate  
 93 on the crater wall in which gullies have incised, key morphological attributes of the substrate, and IDs of HiRISE imagery and  
 94 DTM used for morphological and morphometric investigation of gullies in these craters.

Crater	Latitude	Longitude	No. of gullies	Substrate	Key morphological attributes	HiRISE ID	HiRISE DTM ID
Artik	34.8° S	131.02° E	2	LDM/glacial deposits	Polygons, V-shaped incisions, arcuate ridges, small-scale LDAs on the floor	ESP_020740_1450	DTEEC_012459_1450_012314_1450_A01
Asimov	47.53° S	4.41° E	4	LDM/glacial deposits	Polygons, V-shaped incisions, mantled alcoves/channels/fans, arcuate ridges, small-scale LDAs inside valleys	ESP_012912_1320	DTEEC_012912_1320_012767_1320_A01
Bunnik	38.07° S	142.07° W	8	LDM/glacial deposits	Polygons, V-shaped incisions, mantled alcoves/channels/fans, arcuate ridges	ESP_047044_1420	DTEEC_002659_1420_002514_1420_U01
Corozal	38.78° S	159.48° E	6	LDM/glacial deposits	Polygons, mantled alcoves/channels/fans, arcuate ridges, small-scale LDAs on the floor	PSP_006261_1410	DTEEC_006261_1410_014093_1410_A01
Dechu	42.23° S	158° W	8	LDM/glacial deposits	Polygons, mantled alcoves/channels/fans, arcuate ridges, small-scale LDAs on the floor	PSP_006866_1375	DTEED_023546_1375_023612_1375_A01
Dunkassa	37.46° S	137.06° W	5	LDM/glacial deposits	Polygons, V-shaped incisions, mantled alcoves/channels/fans, arcuate ridges, small-scale LDAs on the floor	ESP_032011_1425	DTEEC_039488_1420_039343_1420_A01
Hale	35.7° S	36.4° W	8	LDM/glacial deposits	Polygons, V-shaped incisions, mantled alcoves/channels/fans, talus slope deposits	PSP_003209_1445	DTEEC_002932_1445_003209_1445_A01
Langtang	38.13° S	135.95° W	5	LDM/glacial deposits	Polygons, V-shaped incisions, mantled alcoves/channels/fans, arcuate ridges, small-scale LDAs on the floor	ESP_030099_1415	DTEEC_024099_1415_023809_1415_U01

Moni	46.97° S	18.79° E	5	LDM/glacial deposits	Partly infilled alcoves, mantled fan surfaces, arcuate ridges	ESP_056862_1325	DTEEC_007110_1325_006820_1325_A01
Nybyen	37.03° S	16.66° W	8	LDM/glacial deposits	Polygons, mantled alcoves/channels/fans, arcuate ridges	ESP_059448_1425	DTEEC_006663_1425_011436_1425_A01
Palikir	41.56° S	157.87° W	5	LDM/glacial deposits	Polygons, V-shaped incisions, mantled alcoves/channels/fans, arcuate ridges, small-scale LDAs on the floor	ESP_057462_1380	DTEEC_005943_1380_011428_1380_A01
Penticton	38.38° S	96.8° E	7	LDM/glacial deposits	Polygons, V-shaped incisions, mantled alcoves/channels/fans, arcuate ridges, small-scale LDAs on the floor	ESP_029062_1415	DTEEC_001714_1415_001846_1415_U01
Selevac	37.37° S	131.07° W	8	LDM/glacial deposits	Polygons, mantled alcoves/channels/fans, small-scale flows on the floor	ESP_045158_1425	DTEEC_003252_1425_003674_1425_A01
Raga	48.1° S	117.57° W	4	LDM	Polygons, mantled alcoves/channels/fans	ESP_041017_1315	DTEEC_014011_1315_014288_1315_A01
Roseau	41.7° S	150.6° E	1	LDM	Polygons, mantled alcoves/channels/fans	ESP_024115_1380 / ESP_011509_1380	ESP_024115_1380_ESP_011509_1380*
Taltal	39.5° S	125.8° W	7	LDM/glacial deposits	Polygons, V-shaped incisions, mantled alcoves/channels/fans, arcuate ridges, small-scale LDAs on the floor	ESP_037074_1400 / ESP_031259_1400	ESP_037074_1400_ESP_031259_1400*
Talu	40.34° S	20.11° E	7	LDM/glacial deposits	Polygons, V-shaped incisions, mantled alcoves/channels/fans, arcuate ridges, small-scale LDAs on the floor	ESP_011817_1395	DTEEC_011817_1395_011672_1395_O01
Triolet	37.08° S	168.02° W	4	LDM/glacial deposits	Polygons, V-shaped incisions, mantled alcoves/channels/fans, arcuate ridges, small-scale LDAs on the floor	ESP_047190_1425	DTEEC_023586_1425_024008_1425_A01
Unnamed crater	32.31° S	118.55° E	4	LDM/glacial deposits	Polygons, mantled alcoves/channels/fan	PSP_006869_1475	DTEEC_021914_1475_022336_1475_U01

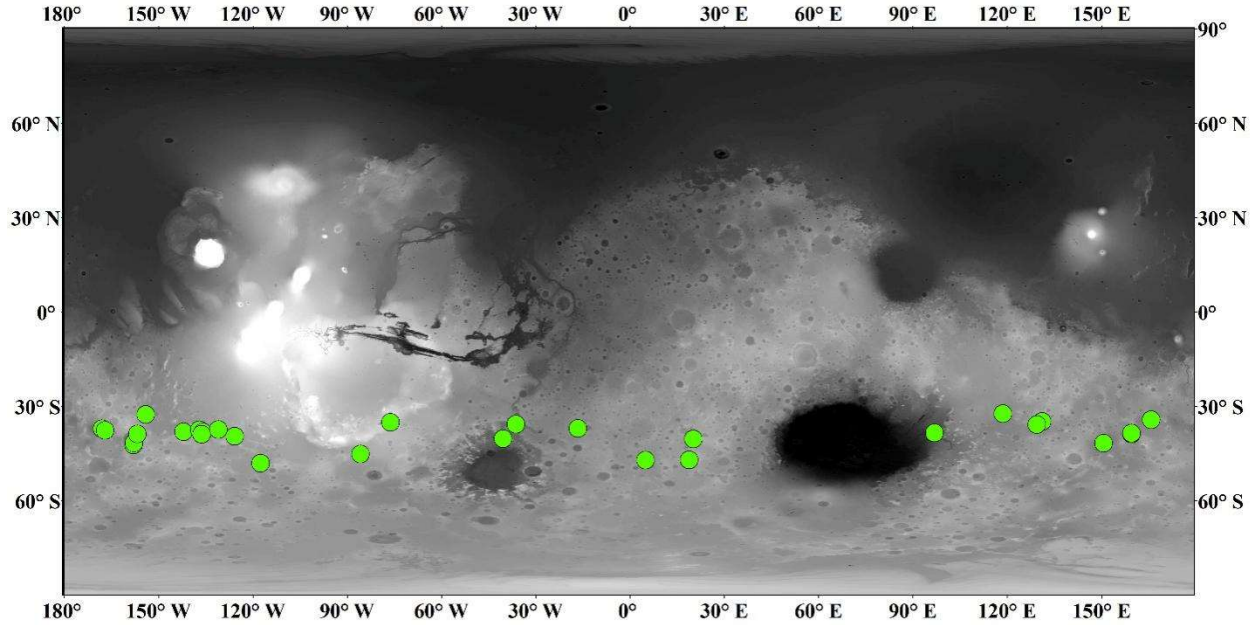
					s, arcuate ridges, small-scale LDAs on the floor		
Unnamed crater in the Argyre basin	40.3° S	40.4° W	6	LDM/glacial deposits	Polygons, mantled alcoves/channels/fans, arcuate ridges, small-scale LDAs on the floor	ESP_032047_1395	DTEEC_012795_1395_013507_1395_A01
Unnamed crater in the Newton basin	38.8° S	156.8° W	5	LDM	Polygons, V-shaped incisions, mantled alcoves/channels/fans	PSP_002686_1410	DTEEC_002620_1410_002686_1410_A01
Unnamed crater north of Corozal crater	38.53° S	159.44° E	5	LDM/glacial deposits	Polygons, mantled alcoves/channels/fans, small-scale LDAs on the floor	ESP_020884_1410	DTEEC_020884_1410_020950_1410_A01
Unnamed crater-1 in the Terra Sirenum	32.55° S	154.11° W	2	LDM	Mantled alcoves/channels/fans	PSP_007380_1470	DTEEC_010597_1470_007380_1470_U01
Unnamed crater-2 in the Terra Sirenum	38.88° S	136.36° W	6	LDM/glacial deposits	Polygons, V-shaped incisions, mantled alcoves/channels/fans, arcuate ridges, small-scale LDAs on the floor	ESP_020407_1410	DTEEC_022108_1410_022385_1410_A01
Istok	45.1° S	85.82° W	8	Bedrock	Alcove cut directly into the original crater-wall material, clasts embedded into fresh deposits on fan	ESP_056668_1345	DTEEC_040607_1345_040251_1345_A01
Galap	37.66° S	167.07° W	8	Bedrock	Alcove cut directly into the original crater-wall material, clasts embedded into fresh deposits on fan	ESP_059770_1420	DTEEC_048983_1420_048693_1420_U01
Gasa	35.73° S	129.4° E	7	Bedrock	Alcove cut directly into the original crater-wall material, clasts embedded into fresh deposits on fan	ESP_057491_1440	DTEEC_021584_1440_022217_1440_A01
Los	35.08° S	76.23° W	7	Bedrock	Alcove cut directly into the original crater-wall material,	ESP_020774_1445 / ESP_050127_1445	ESP_020774_1445_ESP_050127_1445*

					clasts embedded into fresh deposits on fan		
Unnamed crater-3 in the Terra Sirenum	34.27° S	165.71° E	7	Bedrock	Alcove cut directly into the original crater-wall material, clasts embedded into fresh deposits on fan	ESP_049261_1455 / ESP_049828_1455	ESP_049261_1455_ ESP_049828_1455*

95

96 (\*) DTMs are produced with the software packages USGS ISIS and BAE Systems SocetSet.

97



98 Figure 1: Locations of craters analyzed in this study (green circles). Background: Mars Orbiter Laser Altimeter gridded data, where  
 99 white is high elevation and black is low elevation, credit MOLA Science Team/NASA/JPL.

100

### 101 3 Approach

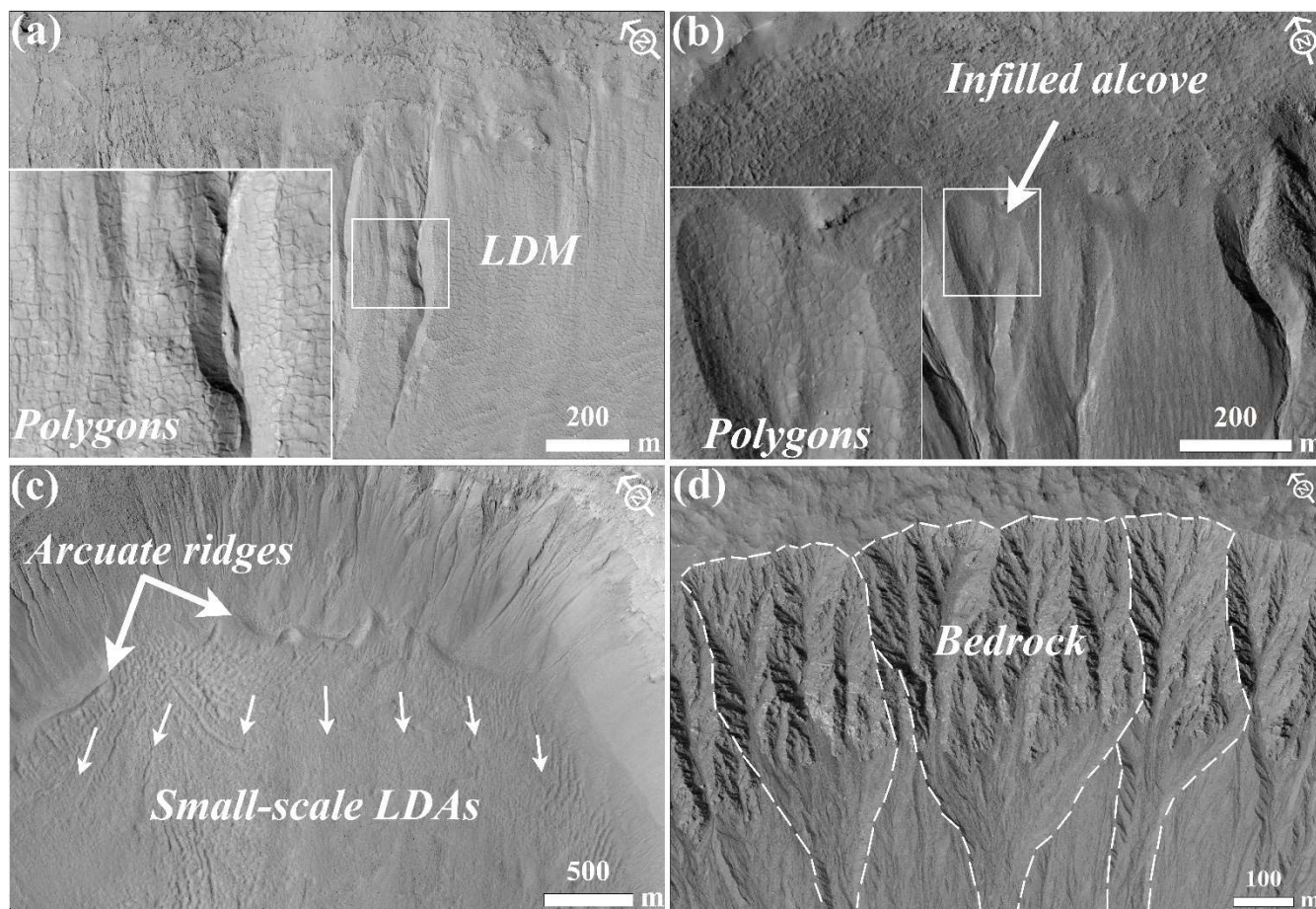
#### 102 3.1 Identification of substrate

103 The substrate into which the gullies have incised is identified based on the following criteria:

- 104 1. LDM/glacial deposits: Any crater whose gullies incise walls that appear to be softened by the drape of smooth mantling  
 105 material with polygonal cracks is inferred to have LDM as the substrate within which gullies have incised (e.g. Mustard et al.,

106 2001; Kreslavsky and Head, 2002; Levy et al., 2009a; Conway et al., 2018; de Haas et al., 2019a) (Fig. 2a-b). The gully alcoves  
107 on the walls of these craters may be partially to completely filled by LDM, and in some cases, polygonized LDM materials  
108 may be seen covering the alcove walls (e.g. Christensen, 2003; Conway et al., 2018; de Haas et al., 2019a). These infilled  
109 alcoves on the crater walls are not the alcoves of gullies formed within the LDM substrate; instead, they represent the alcoves  
110 that were formed prior to the LDM emplacement epoch. Additionally, gullied craters that show evidence in the form of arcuate  
111 ridges at the foot of the walls and VFFs that cover part or the entire crater floor are inferred to have been modified by one or  
112 multiple episodes of glaciation (e.g. Arfstrom and Hartmann, 2005; Head et al., 2010; Milliken et al., 2003; Hubbard et al.,  
113 2011) (Fig. 2c). These craters host gullies that are often partially or fully covered by LDM deposits and are also inferred to  
114 incise LDM deposits.

115 2. Bedrock: Craters where the features listed in criterion 1 (LDM/glacial deposits) are absent and where rocky material is  
116 visible extending downwards from the crater rim (Fig. 2d). This rocky material usually outcrops as spurs and can be layered  
117 or massive. The slopes can be smooth or covered with boulders, with concentrations of boulders at the slope toe.



118

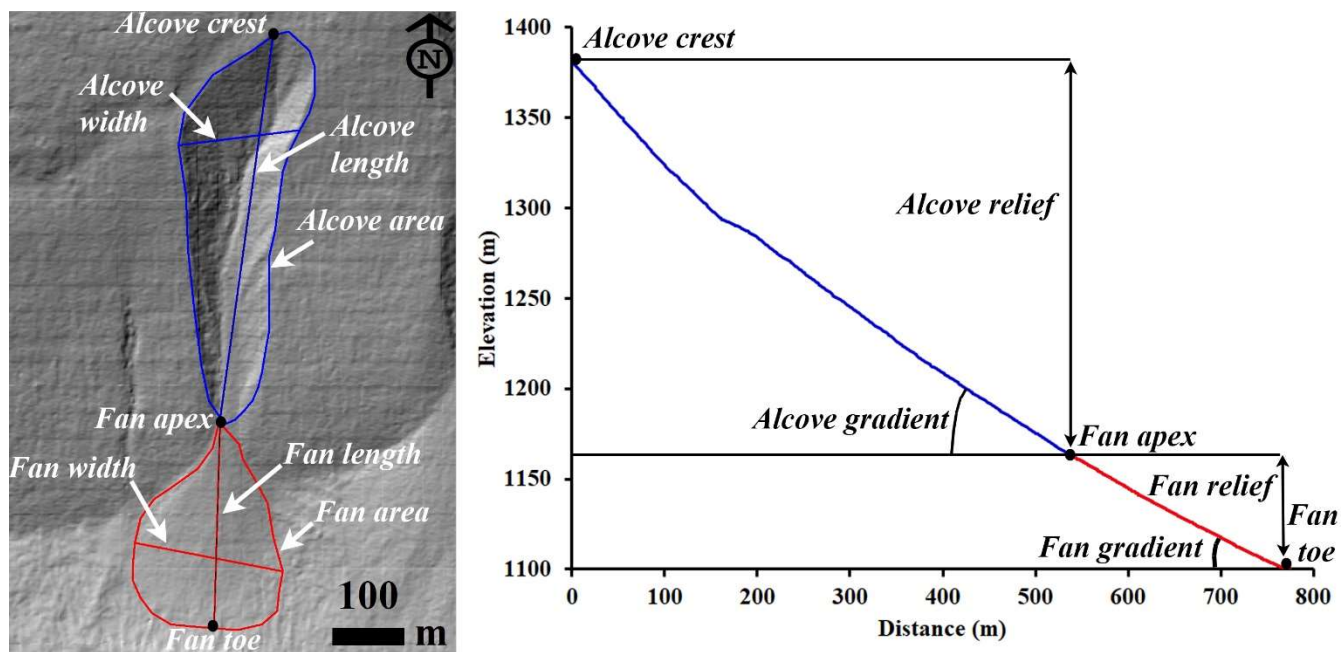


119 Figure 2: Examples of morphological evidence used to identify LDM, glacial deposits, and bedrock. (a) Smooth mantling material  
 120 inferred as LDM draped on the wall of Talu crater on the basis of polygonal cracks formed in the material. The bigger box is an  
 121 expanded view of the polygons seen over the region outlined by the smaller box. (HiRISE image ESP\_011817\_1395). (b) An infilled  
 122 alcove on the wall of an unnamed crater-2 in Terra Sirenum. Polygons in the infilled material suggests presence of LDM deposits  
 123 draped on the wall. The region shown in smaller box is expanded in the bigger box to show evidence of the polygons. (HiRISE image  
 124 ESP\_020407\_1410). (c) Glaciation inferred in the Corozal crater on the basis of arcuate ridges formed at the foot of the crater wall  
 125 and small-scale LDAs on the crater floor. Arrows indicate the downslope flow of LDAs on the floor. (HiRISE image  
 126 PSP\_006261\_1410). (d) Exposed fractured bedrock identified on the walls of Istok crater within which gully alcoves have incised.  
 127 The dashed lines show the gully systems that were investigated in this study. (HiRISE image ESP\_056668\_1345). HiRISE image  
 128 credit: NASA/JPL /University of Arizona.

129

### 130 3.2 Morphometric variables

131 The measurements we made of each gully system include alcove area, alcove perimeter, alcove length, alcove width, alcove  
 132 gradient, fan area, fan length, fan width, and fan gradient (Fig. 3). In total, we derived 18 morphometric variables to  
 133 characterize each gully fan and its alcove. The morphometric variables are classified into geometry, relief, gradient, and  
 134 dimensionless variables (e.g. form factor, elongation ratio, and circularity ratio) and they are calculated with established  
 135 mathematical equations shown in Table 2. For the gradient measurement using the DTM, the topographic profile from (1) crest  
 136 of the alcove to the apex of the fan was extracted for the alcove, and (2) apex to foot of the fan was extracted for the fan.



137

138 Figure 3: Examples of morphometric variables estimated in this work. Left panel: HiRISE DTM (Id:  
 139 DTEEC\_002659\_1420\_002514\_1420) based hillshade. HiRISE DTM credit: NASA/JPL /University of Arizona. Right panel:

140 **Topographic profile: blue profile represents the topography of gully alcove from alcove top to fan apex and red profile represents**  
 141 **the profile of gully fan from fan apex to fan toe.**

142

143

144 **Table 2.** Set of morphometric variables extracted from the studied gully systems and their formulas and/or description of  
 145 method.

<b>Morphometric variable</b>	<b>Formula and/or description of method</b>	<b>References</b>
Alcove length and width	Measured in km	<b>Tomczyk, 2021</b>
Alcove area	Measured in km <sup>2</sup>	<b>Tomczyk, 2021</b>
Fan length and width	Measured in km	<b>Tomczyk, 2021</b>
Fan area	Measured in km <sup>2</sup>	<b>Tomczyk, 2021</b>
Melton ratio	(Alcove relief)/(Alcove area <sup>-0.5</sup> )	<b>Melton, 1957</b>
Relative concavity index (RCI)	Concavity Index/(maximum relief between the uppermost and lowermost points along the gully fan profile/2). Concavity Index is estimated as $\sum (H_i^* - H_i) / N$ , where $H_i^*$ is the elevation along the straight line, $H_i$ is the elevation along the gully fan profile, $N$ is the total number of measurement points.	<b>Langbein, 1964; Phillips and Lutz, 2008</b>
Alcove gradient	Measured in (°)	<b>Tomczyk, 2021</b>
Fan gradient	Measured in (°)	<b>Tomczyk, 2021</b>
Alcove relief	Measured in km	<b>Tomczyk, 2021</b>
Fan relief	Measured in km	<b>Tomczyk, 2021</b>
Relief ratio (alcove and fan)	Alcove/fan relief divided by the length of the alcove/fan	<b>Schumm, 1956a, b</b>
Alcove Perimeter	Measured in km	<b>Schumm, 1956a, b</b>
Form factor	Alcove area divided by the square of the length of the alcove	<b>Horton, 1932</b>
Elongation ratio	Diameter of a circle of the same area as the alcove divided by the maximum alcove length	<b>Schumm, 1956a, b</b>
Circularity ratio	Alcove area divided by the area of the circle having the same perimeter as the alcove perimeter	<b>Miller, 1953</b>

146

### 147 **3.3 Gully system selection for morphometric measurements**

148 We have selected only those gully systems for morphometric measurements in which: (i) the depositional fan from an alcove-  
 149 channel system is not superimposed by or interfingering with the fans from the neighboring channels, (ii) there is clear  
 150 association between the primary channel emanating from the alcove that extends downslope and then deposit its respective  
 151 fan, (iii) no evidence of extensive cross-cutting is seen with the neighboring channels on the walls, (iv) no evidence of extensive  
 152 mantling by dust/aeolian deposits is apparent, and (v) no evidence of channel/fan superposition on any topographic obstacle  
 153 on the walls or the floor of the crater is apparent, which may have influenced the morphometry. If in any case the fans

154 superimpose or channels cross-cut, we have carefully demarcated the alcove-channel-fan boundary, to minimize the  
155 inaccuracies in the measurements. Note that the selection of the gully systems was also constrained by the coverage of HiRISE  
156 DTMs used for morphometric analysis.

### 157 **3.4 Statistical analysis of morphometric variables**

158 We have two groups of gullies in our study: (1) gullies whose source areas are incised into LDM/glacial deposits and (2)  
159 gullies whose source areas are incised into the bedrock. First, for both the groups we have calculated descriptive statistics for  
160 each of the morphometric variables shown in Table 2. The significance of the difference between the values of each of the  
161 morphometric variables calculated for each group was tested using a Student's t-test. To apply t-tests, we have transformed  
162 the morphometric variables to remove skewness by taking their natural logarithm. Pearson correlation analysis has been used  
163 to investigate the correlation between the selected morphometric attributes of gully alcoves and fans. We infer strong positive  
164 correlations between variables if the correlation coefficient value is more than 0.7 and strong negative correlations if the value  
165 is less than -0.7. Very strong positive correlation between variables is inferred if the correlation coefficient is  $\geq 0.9$ . Further,  
166 we used canonical discriminant analysis (CDA) to determine morphometric variables that provide the most discrimination  
167 between the groups of gullies. In CDA, functions are generated according to the number of groups, until a number equal to n-  
168 1 functions is reached (n is the number of groups) (McLachlan, 2005). For the two groups of gullies in our study, there is going  
169 to be a function for which there is a standardised canonical discriminant function coefficient associated with the morphometric  
170 variable. The higher the magnitude of this coefficient for a particular morphometric variable, the higher the role of that variable  
171 in separating the groups of gullies (Conway et al., 2015). Standardisation was done by dividing each value for a given variable  
172 by the maximum value.

## 173 **4 Results**

### 174 **4.1 Morphology of gully systems**

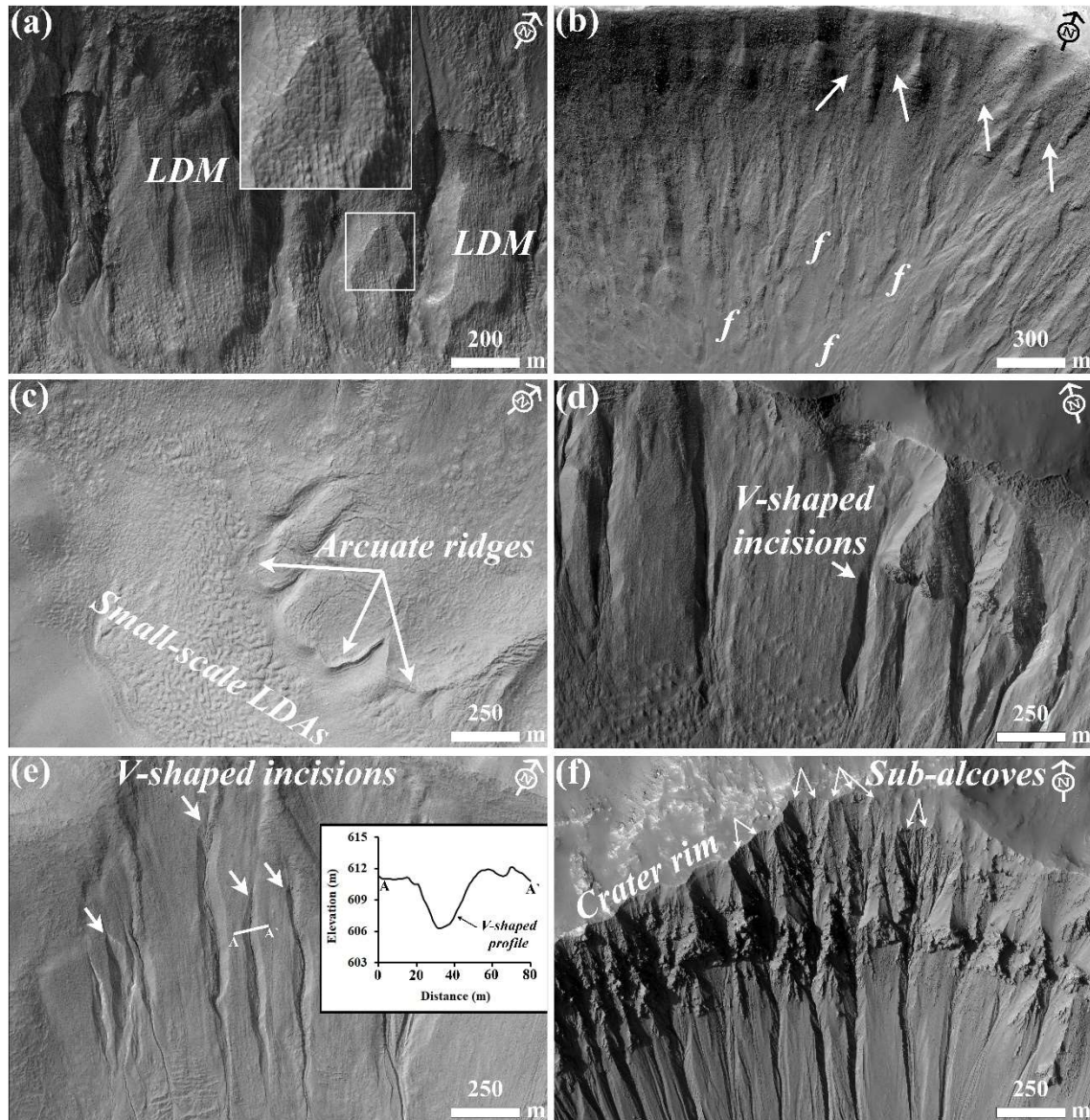
175 Out of the 29 gullied craters analysed in this work, we have found that there are 24 craters influenced by LDM and/or VFFs.  
176 The remaining 5 craters have gullies incised into the exposed underlying bedrock on the wall of the crater. Below we describe  
177 the substrates identified in the studied craters and then compare the morphology of the gullies formed into those substrates.

178 4 craters out of 24 craters (i.e. Raga, Roseau, unnamed crater in Newton basin and unnamed crater-1 in Terra Sirenum) have  
179 gullies that are only influenced by LDM. In these craters, we have found morphological evidence of LDM in the form of  
180 polygonized, smooth textured material on the pole-facing walls of the craters. Morphological evidence of VFF is not evident  
181 in these craters. In these craters, the gully-alcoves and gully channels appear to have been incised into the polygonized LDM  
182 material, and the gully-fan deposits are mantled. A typical example of this can be found in the unnamed crater formed inside  
183 the Newton basin (Fig. 4a). Roseau crater, in particular, contains a large number of gully systems whose alcoves and fans are

184 extensively mantled (Fig. 4b). The remaining 20 out of 24 craters contain evidence for gullies that are influenced by both LDM  
185 and glacial deposits (Table 1). The base of the pole-facing walls and the floor of the craters within which the gully systems  
186 have formed host linear-to-sinuuous arcuate ridges and VFFs, respectively. Typical examples of VFFs can be found in Corozal,  
187 Talu, unnamed craters in Terra Sirenum and Argyre basin, Langtang, Dechu and Dunkassa craters (Fig. 4c). In majority of the  
188 gullied craters (except Raga, Roseau and unnamed crater-1 in Terra Sirenum) influenced by LDM and glacial deposits, gully  
189 alcoves are found to have a distinctive V-shaped cross section in their mid-section (Figures 4d and 4e), they do not extend up

190 to the crater rim, and gully systems often show multiple episodes of activity, inferred by the presence of fresh channel incision  
191 on the gully-fan surfaces (Fig. 4d-e).

192 Istok, Galap, Gasa, Los, and an unnamed crater in the Terra Sirenum contain gully systems on the pole-facing walls that are  
193 not associated with LDM and VFFs (Table 1). The gully alcoves inside these craters have a crenulated shape and appear to  
194 have formed by headward erosion into the bedrock of the crater rim (Fig. 4f). These craters have formed large gully systems  
195 on their pole-facing walls, with brecciated alcoves, comprising of multiple sub-alcoves and hosting many clasts/boulders (Fig.  
196 4f).



214 **Figure 4: (a) LDM draped on the wall of an unnamed crater in the Newton basin. The inset shows details of the polygonal texture of**  
215 **the LDM. (HiRISE image PSP\_002686\_1410). (b) Infilled gully alcoves (arrows) and mantled fan surfaces (marked by letter ‘f’) on**  
216 **the wall of Roseau crater. (HiRISE image ESP\_024115\_1380). (c) Arcuate ridges at the foot of the crater wall and small-scale LDAs**  
217 **on the floor in Langtang crater. (HiRISE image ESP\_030099\_1415). (d) V-shaped incisions on the LDM draped walls of Taltal**  
218 **(HiRISE image ESP\_037074\_1400) and (e) Langtang crater (HiRISE image ESP\_030099\_1415). Note the topographic profile (A-A’)**  
219 **that illustrates V-shaped incision of the gully channel. (f) Gully alcoves formed in Los crater by headward erosion into the crater**  
220 **rim. Individual gully alcoves formed in bedrock have multiple sub-alcoves. (HiRISE image ESP\_020774\_1445).**

221

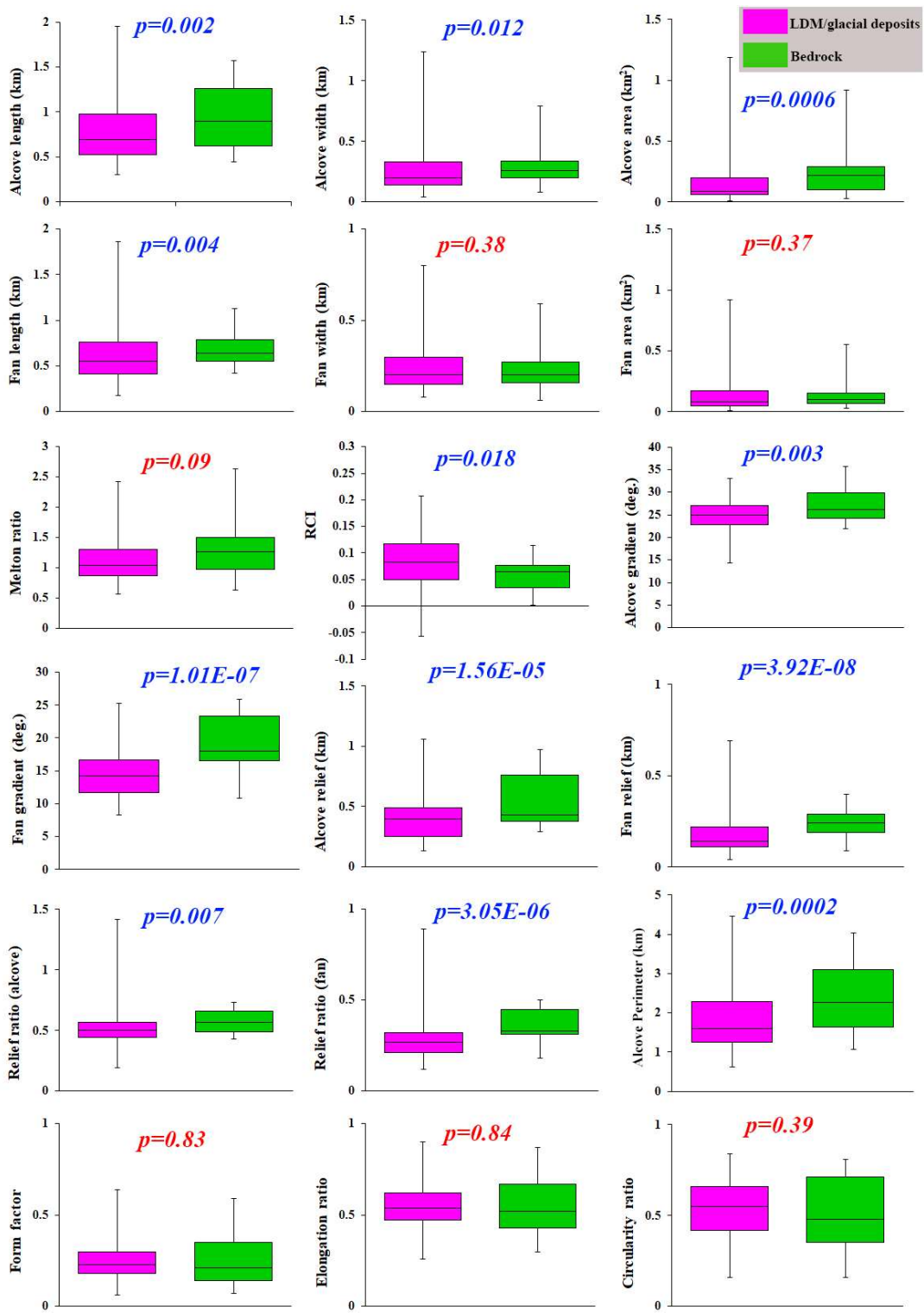
## 222 **4.2 Morphometry of gully systems**

223 Based on the criteria summarized in section 3.3, we have studied 167 gullies across 29 craters for calculation of morphometric  
224 variables. 130 gullies are formed within LDM/glacial deposits, and 37 gullies are formed within the bedrock. The results of  
225 morphometric calculations are summarized for visual comparison as a boxplot (Fig. 5).

226 The results of the Student’s t-test indicates that all of the morphometric variables in Table 2, except fan width, fan area, Melton  
227 ratio, form factor, elongation ratio, and circularity ratio, differ significantly between LDM/glacial deposits and bedrock (Fig.  
228 5). Compared to the mean gradient of gully-fans formed in LDM/glacial deposits, bedrock gully-fans are steeper and possess  
229 a higher relief ratio. The interquartile range of length, relief, and perimeter of gully alcoves formed in bedrock are also higher  
230 than the interquartile range of similar variables in LDM/glacial deposits, but the gully alcoves in LDM/glacial deposits possess  
231 much higher values of length, relief, and perimeter (Fig. 5).

232

233  
 234  
 235  
 236  
 237  
 238  
 239  
 240  
 241  
 242  
 243  
 244  
 245  
 246  
 247  
 248  
 249  
 250  
 251  
 252  
 253  
 254  
 255  
 256  
 257  
 258  
 259  
 260



261 **Figure 5: The boxplot presented here shows interquartile range, central horizontal bar shows median, and whiskers show range of**  
262 **values of alcove/fan geometry, relief, gradient, and dimensionless variables of gullies incised into LDM/glacial deposits (pink) and**  
263 **bedrock (green). P-values on the plots represent the results of the student's t-tests for testing the significance of difference in means**  
264 **of the morphometric variables between gully systems formed on LDM/Glacial deposits and bedrock. P-values in blue correspond to**  
265 **significant difference (with respect to a p-value of 0.05) and those in red are non-significant.**

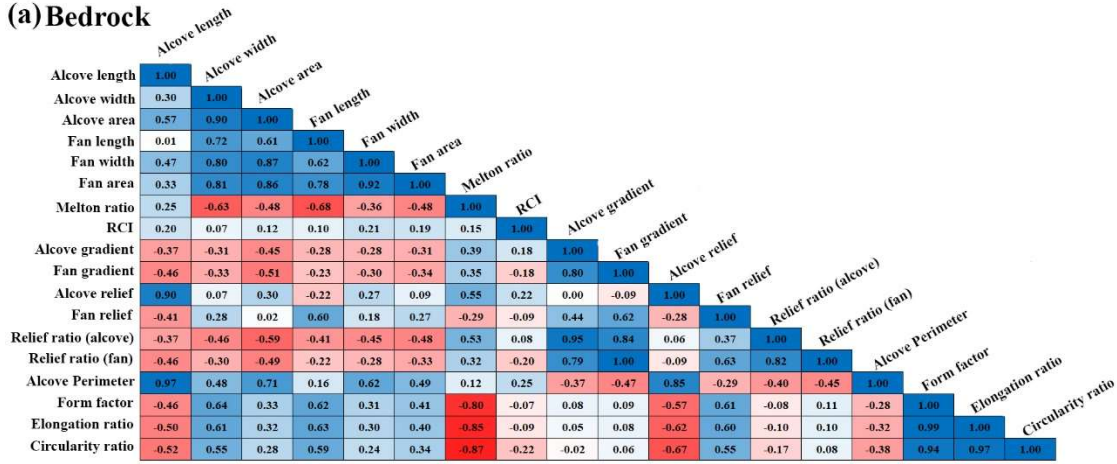
266

267 Pearson correlations between morphometric attributes of gully alcoves and fans formed in bedrock and LDM/glacial deposits  
268 are summarized in Fig. 6. For bedrock, there are strong positive correlations between 12 pairs of morphometric variables and  
269 strong negative correlations between 3 pairs of morphometric variables. For LDM/glacial deposits, there are strong positive  
270 correlations between 18 pairs of morphometric variables and strong negative correlations between 3 pairs of morphometric  
271 variables. Very strong positive correlations ( $>0.9$ ) are found between 9 pairs of morphometric variables for bedrock and  
272 between 4 pairs of morphometric variables for LDM/glacial deposits.

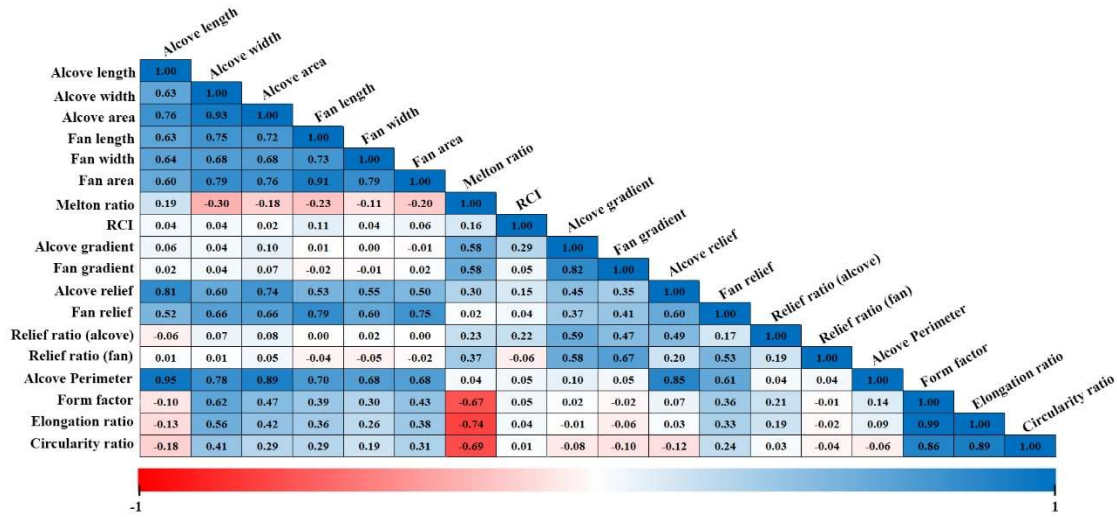


273

(a) Bedrock



(b) LDM/glacial deposits



284

285

286

287

288

289

290

291

292

293

294

295 **Figure 6: Pearson correlations between morphometric attributes of gully alcoves and fans formed in (a) bedrock and (b) LDM/glacial**  
 296 **deposits. Values approaching either 1 or -1 have stronger correlations. Zero indicates no correlation.**

297

298 The canonical discriminant analysis reveals that the following morphometric variables best distinguish between the gully  
 299 systems formed in LDM/glacial deposits and bedrock, in descending order of importance: alcove perimeter, alcove relief, fan  
 300 gradient, fan relief, fan length, relief ratio (alcove), alcove width, relief ratio (fan), alcove gradient, alcove area, alcove length,  
 301 and relative concavity index (Table 3). The alcove perimeter is most important in discriminating among the gully systems  
 302 formed within LDM/glacial deposits and bedrock, and the next two most important variables are alcove relief and fan gradient.  
 303 Alcove relief and fan gradient have 4/5 and 1/3 the weight of alcove perimeter, respectively. Here, the weight values indicate

304 the discriminator power in separating between the gullies formed in LDM/glacial deposits and bedrock. The remaining  
 305 variables such as fan relief, fan length, relief ratio (alcove), alcove width, and relief ratio (fan) have nearly 1/5 or greater (but  
 306 less than 1/3) of the weight of alcove perimeter discriminatory power in separating between the gullies formed in LDM/glacial  
 307 deposits and bedrock. The variables with the smallest magnitude, alcove gradient, alcove area, alcove length and relative  
 308 concavity index, have less than 1/10 the weight of the most important variable in separating the gully systems.

309 **Table 3.** Standardised canonical discriminant function coefficients (F1) that best separate gully systems formed on  
 310 LDM/Glacial deposits and bedrock.

<b>Variable</b>	<b>F1</b>
Alcove Perimeter	3.552
Alcove relief	-2.828
Fan gradient	1.278
Fan length	-1.06
Fan relief	1.06
Relief ratio (alcove)	0.971
Alcove width	-0.692
Relief ratio (fan)	-0.665
Alcove gradient	-0.331
Alcove area	-0.319
Alcove length	0.23
Relative concavity index	-0.182

311

## 312 **5 Discussion**

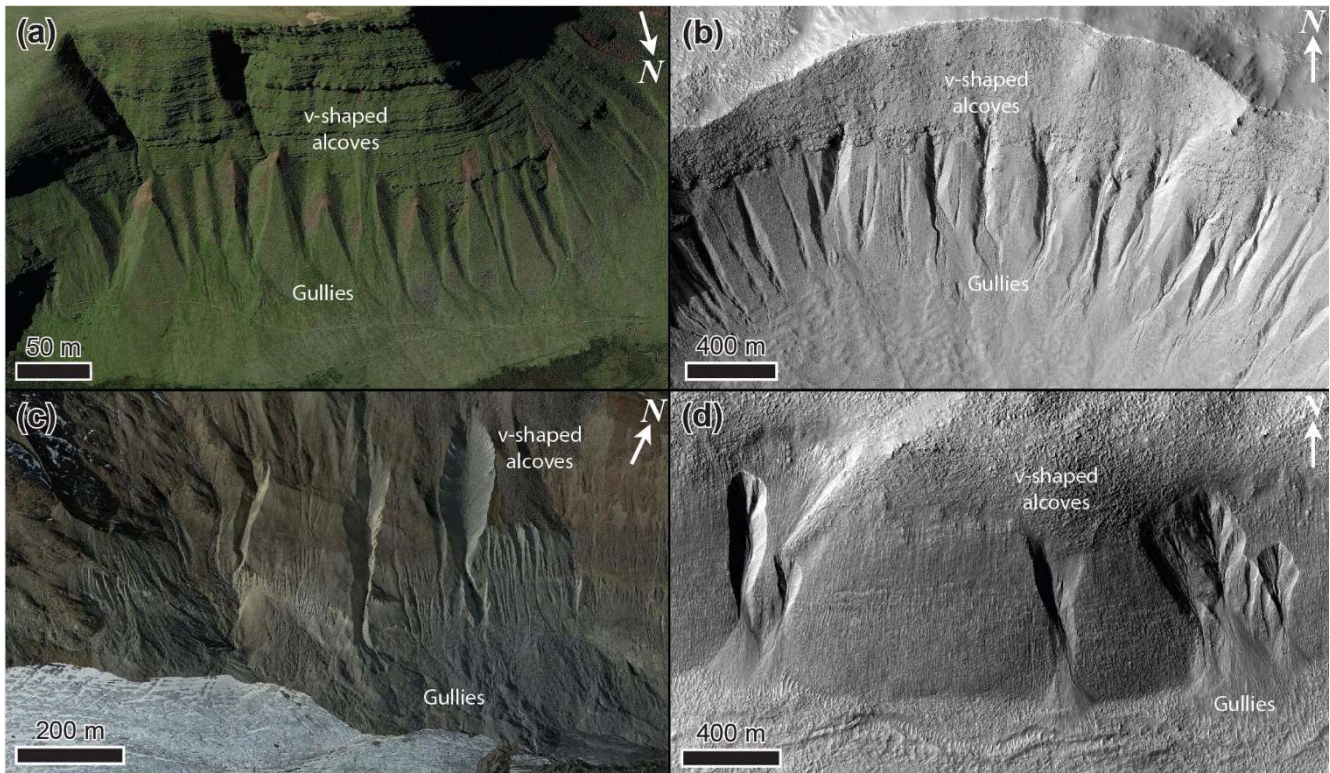
### 313 **5.1 Unique morphology and morphometry of gully systems in different substrates**

314 We have found that the gully systems formed in LDM/glacial deposits and bedrock can, using discriminatory analysis, be  
 315 distinguished from one another in terms of perimeter and relief of gully alcoves (Table 3). Additionally, we have found  
 316 statistically significant difference between the perimeters and reliefs of gully alcoves formed in LDM/glacial deposits and  
 317 bedrock (Fig. 5). It is likely that these differences in the perimeters and reliefs of gully alcoves formed within morphologically  
 318 distinct substrates could be due to the integral nature of the surface material within which the gully alcoves have formed. In  
 319 other words, it is possible that the differences in the physical properties of the sediments (namely grain size, compactness etc.)  
 320 within which gully alcoves have formed played a key role in erosion of the substrate leading to differences in their

321 morphometric variables. Below we elaborate on the uniqueness of the substrates within which gully alcoves have formed, and  
322 discuss further the relationships between the morphometric variables of the morphologically distinct gully systems.

323 On Mars, VFFs contain high purity glacial ice with a debris cover (Sharp, 1973; Squyres, 1978, 1979; Squyres and Carr, 1986;  
324 Holt et al 2008, Plaut et al 2009, Petersen et al. 2018). Their surfaces have been interpreted to comprise of finer, reworked  
325 debris derived from sublimation of the underlying ice (Baker et al., 2010; Plaut et al., 2009). The smooth, meters thick draping  
326 unit on the walls of formerly glaciated craters has been suggested to be derived from the atmosphere as a layer of dust-rich ice  
327 primarily constituting of fine-grained materials (Kreslavsky and Head, 2000; Mustard et al., 2001). The fine-grained materials  
328 are loosely-packed, unconsolidated materials exhibiting low thermal inertia values (Mellon et al., 2000; Putzig et al., 2005).  
329 Typically, gullies formed within this substrate display a smooth surface texture, wherein, evidence of individual clasts or  
330 meter-scale boulders is not resolvable in HiRISE images, substantiating the dominant component of fine-grained materials  
331 within the LDM (e.g., Levy et al., 2010; de Haas et al., 2015a). Additionally, it has been found that gully alcoves incised into  
332 the LDM always have a distinctive V-shaped cross section in their mid-section (Figures 4d and 4e), which when compared  
333 with similar-scaled systems on Earth also corresponds to the presence of loose sediments constituting the LDM (Conway et  
334 al., 2018). The gully alcoves with V-shaped cross sections are found to be elongated, likely indicating incision within ice-rich  
335 unlithified sediments (Aston et al., 2011). In the studied craters, we have found that gullies incised into LDM/glacial deposits  
336 do have an elongated, V-shaped cross section in their mid-sections (Fig. 4). We propose that the presence of fine-grained,  
337 loosely packed, unconsolidated materials within LDM/glacial deposits has facilitated formation of elongated gully alcoves  
338 with perimeters and reliefs relatively higher than that of gully alcoves formed in coarse-grained bedrock substrate. This is  
339 consistent with the previous studies suggesting that gullies eroding into LDM/glacial deposits have elongated catchments  
340 (Aston et al., 2011), whereas gullies eroding into the bedrock have more amphitheater-shaped catchments (Levy et al., 2009b).  
341 For this reason, the estimated length of gully alcoves formed in LDM/glacial deposits is found to be relative higher than that  
342 of gully alcoves formed in bedrock (Fig. 5). Furthermore, statistical analysis has revealed a significant difference between the  
343 length of gully alcoves formed in LDM/glacial deposits and bedrock (Fig. 5). Additionally, the presence of finer-grained  
344 sediments in LDM/glacial deposits is the likely cause of the V-shape of the incision of gully alcoves investigated in this study  
345 (Aston et al., 2011). On Earth, V-shaped incisions through glacial ice-rich moraines have been observed to have occurred  
346 during the paraglacial phase of glacial retreat (Bennett et al., 2000; Ewertowski and Tomczyk, 2015) (Fig. 7). The paraglacial  
347 phase refers to a terrestrial post-glacial period that represents the response of changing environment to deglaciation (Bennett  
348 et al., 2000; Ewertowski and Tomczyk, 2015).

349



350

351 **Figure 7: Gullies forming in glacial sediments in deglaciated terrain in the (a) Brecon Beacons, Wales, UK on Earth (Google Earth**  
 352 **coordinates: 51°52'59.11"N, 3°43'33.26"W), (b) Talu crater ([https://www.uahirise.org/ESP\\_011817\\_1395](https://www.uahirise.org/ESP_011817_1395)) on Mars, (c)**  
 353 **Hintereisferner, Austria (Google Earth coordinates: 46°48'54.25"N, 10°47'8.18"E), on Earth, and (d) Bunnik crater**  
 354 **([https://www.uahirise.org/ESP\\_047044\\_1420](https://www.uahirise.org/ESP_047044_1420)) on Mars. HiRISE image credit: NASA/JPL-Caltech/University of Arizona.**

355

356 The next most important difference between these two types of gullies is the mean gradient of gully fans. At the foot of the  
 357 fans, mean gradient of the fans influenced by LDM/glacial deposits is  $<15^\circ$  for 61% of the studied fans. For bedrock, 84% of  
 358 the studied fans have a mean gradient  $>15^\circ$  at the foot of the fans. Hence, gully-fans formed in bedrock are emplaced at a  
 359 relatively steeper gradient than the fans formed from gullies in LDM/glacial deposits. We propose that the nature of the material  
 360 mobilized can explain this difference, with the finer-grained sediments characteristic of the LDM/glacial type gullies being  
 361 easier to mobilise and being entrained to lower slope angles, than the coarser sediments found within the bedrock type gullies.

## 362 5.2 Evaluation of the gully formation process

363 On Earth, alcove-fan systems can roughly be subdivided in flood-dominated, debris-flow dominated, and colluvial systems.  
 364 Following the terminology of De Haas et al., (2015b) and Tomczyk (2021), we define these systems as follows:

365 1) Flood-dominated systems: These are systems dominated by fluid-gravity flows, i.e., water floods, hyperconcentrated floods,  
366 and debris floods. The fans of such systems are commonly referred to as fluvial or alluvial fans (e.g., Ryder, 1971; Blair and  
367 McPherson, 1994; Hartley et al., 2005).

368 2) Debris-flow dominated systems: These are systems dominated by sediment-gravity flows, i.e., debris flows, mud flows.  
369 Irrespective of their radial extent and depositional gradients, the fans aggraded by these systems can be commonly called  
370 debris-flow fans or debris fans (Blikra and Nemeč, 1998; de Scally et al., 2010).

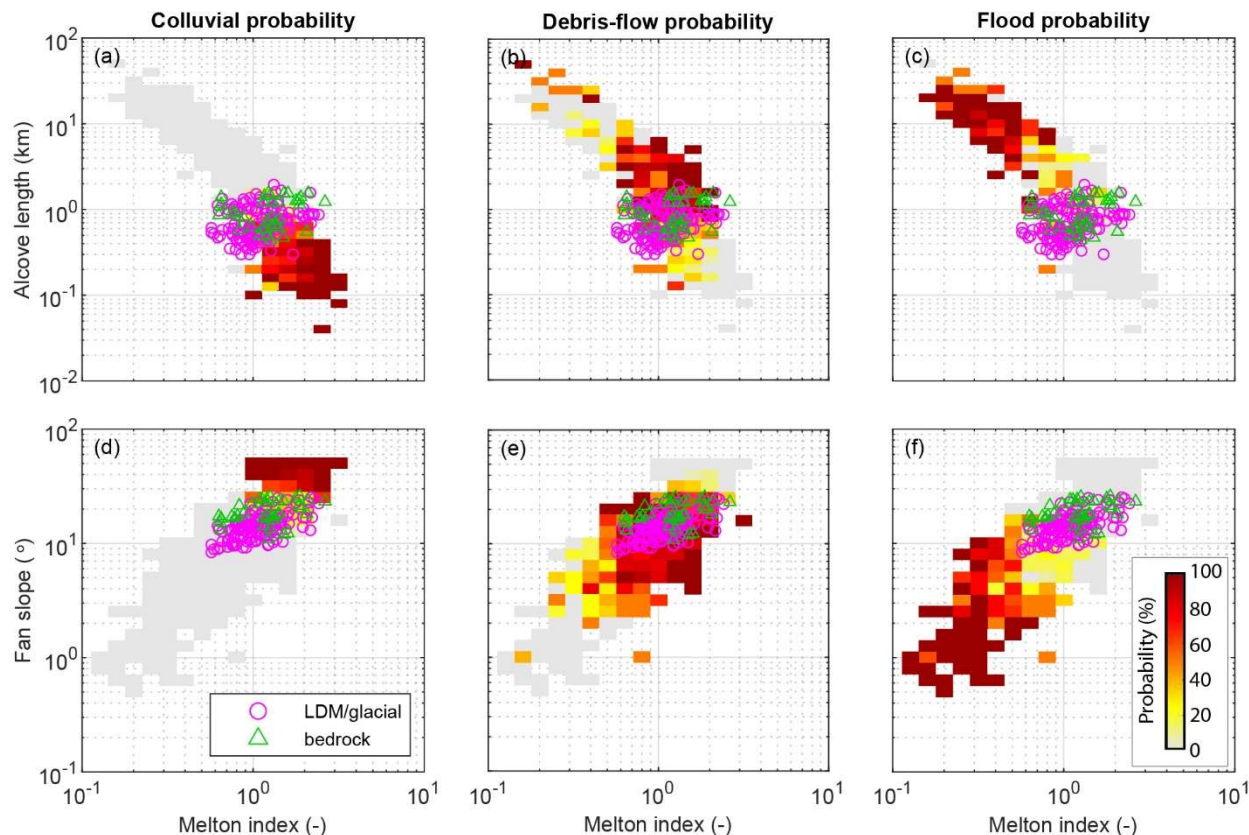
371 3) Colluvial systems: These are systems dominated by rock-gravity and sediment-gravity flows, with their dominant activity  
372 relating to rockfalls, grain flows, and snow avalanches (in periglacial and alpine settings). Debris flows typically constitute  
373 only a relatively minor component of geomorphic processes in such systems. The fans of these systems are also commonly  
374 known as colluvial cones or talus cones (Siewert et al., 2012; De Haas et al., 2015b).

375 Although these systems may be dominated by one type of geomorphic process, it is important to stress that other processes  
376 may also occur. For example, on Earth water floods are not uncommon on many debris-flow dominated systems, while debris-  
377 flow deposits are commonly recognized on colluvial cones.

378

379

380



382

383 **Figure 8: Comparison of combinations of Melton ratio with Alcove length and Fan gradient. The probability heat maps**  
 384 **are based on previously published data – see text for references. The Martian gully systems formed in LDM/glacial**  
 385 **deposits and bedrock are found to be in the debris-flow regime on Earth. The gray area shows the realm of the colluvial,**  
 386 **debris-flow, and fluvial fans together.**

387

388 To compare the morphometric characteristics of the Martian gully systems to terrestrial systems, we have compiled  
 389 morphometric data of gully alcoves and fans across several continents, mountain ranges, climate zones, and process types on  
 390 Earth. This dataset includes published data from the Himalayas, Ladakh, India (Stolle et al., 2013), the tropical Andes,  
 391 Columbia (Arango et al., 2021), Spitsbergen, Svalbard (Tomczyk, 2021), British Columbia, Canada (Kostaschuk, 1986;  
 392 Jackson et al., 1987; and newly presented data), the southern Carpathians, Romania (Ilinca et al., 2021), the Southern Alps,  
 393 New Zealand (De Scally and Owens, 2004; De Scally et al., 2010), the North Cascade Foothills, USA, the European Alps  
 394 (including Switzerland, Italy, France, and Austria), and the Pyrenees (from multiple authors compiled by Bertrand et al., 2013).  
 395 The dataset comprises information from colluvial, debris-flow, and flood (also including debris flood) dominated systems. In

396 total, it contains 231 colluvial systems, 749 debris-flow dominated systems, and 369 flood-dominated systems. In total, data  
397 were compiled for 1349 systems, although not all information was available for all systems, with data availability ranging from  
398 729 sites for alcove length to all 1349 systems for Melton index and process type. Based on this data we have made a heatmap  
399 of the probability of flood, debris-flow, or colluvially-dominated conditions for combinations of Melton ratio with alcove  
400 length and fan gradient, to which we compare the Martian gullies (Fig. 8). We have specifically chosen the combinations of  
401 Melton ratio with alcove length and fan gradient to infer the Martian gully formative mechanism because they have been  
402 widely used in discriminating terrestrial drainage basins and fans prone to flooding from those subject to debris flows, debris  
403 floods and floods (e.g. De Scally and Owens, 2004; Wilford et al., 2004). We have found that the Martian gullies are indeed  
404 in the debris-flow regime on Earth. Moreover, they are closer to the transition to the smaller and steeper colluvial cones than  
405 to transition to flood-dominated fans. As expected, bedrock systems in Fig. 8d-e are closer to the colluvial systems than the  
406 LDM systems.

407

408 According to the previous reports of debris-flow like deposits found in Martian gullies (e.g. Johnsson et al., 2014; Sinha et al.,  
409 2019, 2020), the morphological attributes of debris-flow like deposits typically include overlapping tongue-shaped lobes with  
410 embedded clasts, channels with medial deposits, and channels with clearly defined lateral levees. Although it is still not clear  
411 whether the formation of these deposits in gullies are from sublimation of CO<sub>2</sub> ice or due to meltwater generation. De Haas et  
412 al., (2019b) showed that CO<sub>2</sub> sublimation may lead to flow fluidization on Mars in a manner similar to fluidization by water  
413 in terrestrial debris flows; a concept supported by the recent finding of lobate deposits and boulder-rich levee formation during  
414 the present-day in Istok crater (Table 1) (Dundas et al., 2019). The formation of these morphologically similar deposits during  
415 the present-day is attributed to sublimating CO<sub>2</sub> frost, which likely produces the necessary fluidization likely by gas generated  
416 from entrained CO<sub>2</sub> frost (Dundas et al., 2019). On the basis of these recent reports (De Haas et al., 2019b; Dundas et al., 2019)  
417 and based on our own findings in this study, we argue that a debris-flow like process similar to those operated in the terrestrial  
418 gully systems has likely dominated the flow types that lead to gully formation on Mars. Present-day sublimation of CO<sub>2</sub> ice  
419 on Mars may have provided the necessary flow fluidization for the emplacement of deposits similar to terrestrial debris-flow  
420 like deposits (De Haas et al., 2019b).

## 421 **6 Conclusions**

422 This paper compares morphological and morphometric characteristics of gully alcoves and associated fans formed in  
423 LDM/glacial deposits and bedrock over walls of 29 craters between 30° S and 75° S latitudes on Mars. 5 craters out of 29 have  
424 alcoves-fans formed within the bedrock and remaining 24 craters have alcoves-fans formed within LDM/glacial deposits. From  
425 our analysis of 167 gullies, we posit that gully systems formed in LDM/glacial deposits and bedrock differ from one another  
426 using the following lines of evidence:

427 • Gully alcoves formed in LDM/glacial deposits are more elongated than the gully alcoves formed in bedrock, and possess a  
428 distinctive V-shaped cross section.

429 • The mean gradient of gully-fans formed in bedrock is steeper than the mean gradient of fans formed from gullies in  
430 LDM/glacial deposits.

431 The morphological distinction reported between gullies formed in the bedrock and LDM/glacial deposits signifies that Martian  
432 gullies may have multiple formative environments. We infer that the presence of mantling material could be one of the key  
433 factors in constraining the mechanisms forming Martian gully systems and that presence of LDM would promote formation  
434 of elongated gully alcoves with perimeters and reliefs relatively higher than that of gully alcoves formed in coarse-grained  
435 bedrock substrate.

436 Based on the combinations of Melton ratio with alcove length and fan gradient, we suggest that the gully systems studied in  
437 this work were likely dominated by terrestrial debris-flow like processes during their formation. This is consistent with the  
438 findings reported in previous studies that showed evidence of formation of deposits morphologically similar to terrestrial  
439 debris-flow like deposits, both in the past and during the present-day (e.g., Johnsson et al., 2014; Dundas et al., 2019). The  
440 present-day sublimation of CO<sub>2</sub> ice on Mars is envisaged to provide the necessary flow fluidization for the emplacement of  
441 deposits similar to debris-flow like deposits on Earth (De Haas et al., 2019b).

#### 442 **7 Author contribution**

443 RKS, TDH and SJC conceptualized this work. The methodology was developed by RKS, TDH and SJC. Data curation and  
444 formal analyses were performed by RKS. TDH and AN also contributed in collection of datasets used in this work. RKS, DR,  
445 TDH and SJC contributed to the interpretation of the data and results. RKS wrote the original draft of this paper, which was  
446 reviewed and edited by all authors.

#### 447 **8 Conflict of interest**

448 SJC is a Guest Editor of this special issue (Planetary landscapes, landforms, and their analogues) of ESurf and on the editorial  
449 board for ESurf. The peer-review process was guided by an independent editor, and the authors have also no other competing  
450 interests to declare.

#### 451 **9 Acknowledgements**

452 We are grateful and thank both the anonymous reviewers for thorough assessment of our manuscript and for providing us  
453 constructive comments and suggestions. Thanks to the Editor (Heather Viles) and Associate Editor (Frances E. G. Butcher) at  
454 Earth Surface Dynamics for the editorial handling of the manuscript. We would like to thank the HiRISE team for their work  
455 to produce the images and digital elevation models used in this study, it would have been impossible without them. RKS and



456 DR acknowledge the financial support by the Indian Space Research Organisation, Department of Space, Government of India.  
457 SJC and AN are grateful for the financial support from Région Pays de la Loire, project étoiles montantes METAFLOWS  
458 (convention N° 2019-14294) and also the financial support of CNES in support of their HiRISE work. TdH was supported by  
459 the Netherlands Organisation for Scientific Research (NWO) (grant 016.Veni.192.001). We acknowledge the efforts of team  
460 MUTED to develop an online tool (<http://muted.wwu.de/>) for quick identification of the spatial and multi-temporal coverage  
461 of planetary image data from Mars. All the planetary datasets used in this work are available for free download at the PDS  
462 Geosciences Node Mars Orbital Data Explorer (ODE) (<https://ode.rsl.wustl.edu/mars/>) and <https://www.uahirise.org/>. The  
463 newly-generated DTMs can be downloaded from [https://figshare.com/articles/dataset/Self\\_generated\\_DEMs/21717164](https://figshare.com/articles/dataset/Self_generated_DEMs/21717164).  
464 The measurement datasets can be downloaded from  
465 [https://figshare.com/articles/dataset/Measurement\\_data\\_of\\_gully\\_systems\\_in\\_the\\_southern\\_mid\\_latitudes\\_of\\_Mars/](https://figshare.com/articles/dataset/Measurement_data_of_gully_systems_in_the_southern_mid_latitudes_of_Mars/21717182)  
466 **21717182**. This work is a part of the PhD work of Rishitosh K. Sinha. Director PRL, Head of Planetary Science Division,  
467 PRL, Head of Planetary Remote Sensing Section, PRL, and Director IIT Gandhinagar are gratefully acknowledged for constant  
468 encouragement during the work.

## 469 **References**

- 470 Arango, M. I., Aristizábal, E., & Gómez, F.: Morphometrical analysis of torrential flows-prone catchments in tropical and  
471 mountainous terrain of the Colombian Andes by machine learning techniques, *Natural Hazards*, 105(1), 983-1012, doi:  
472 <https://doi.org/10.1007/s11069-020-04346-5>, 2021.
- 473 Arfstrom, J. & Hartmann, W.K.: Martian flow features, moraine-like ridges, and gullies: terrestrial analogs and  
474 interrelationships, *Icarus*, 174, 321–335, doi: <https://doi.org/10.1016/j.icarus.2004.05.026>, 2005.
- 475 Aston, A., Conway, S. & Balme, M.: Identifying Martian Gully Evolution. In: Balme, M.R., Bargery, A.S., Gallagher, C.J. &  
476 Gupta, S. (eds) *Martian Geomorphology*, Geological Society, London, Special Publications, 356, 151–169, doi:  
477 <https://doi.org/10.1144/SP356.9>, 2011.
- 478 Baker, D. M. H, James W. H., and David R. M.: Flow patterns of lobate debris aprons and lineated valley fill north of Ismeniae  
479 Fossae, Mars: Evidence for extensive mid-latitude glaciation in the Late Amazonian, *Icarus* 207, 186-209, 2010, doi:  
480 <https://doi.org/10.1016/j.icarus.2009.11.017>.
- 481 Balme, M., Mangold, N. Et Al.: Orientation and distribution of recent gullies in the southern hemisphere of Mars: observations  
482 from High Resolution Stereo Camera/Mars Express (HRSC/MEX) and Mars Orbiter Camera/Mars Global Surveyor  
483 (MOC/MGS) data, *J. Geophys. Res.: Planets*, 111, E05001, doi: <https://doi.org/10.1029/2005JE002607>, 2006.
- 484 Bertrand, M., Liébault, F., & Piégay, H.: Debris-flow susceptibility of upland catchments, *Natural Hazards*, 67(2), 497-511,  
485 doi: <https://doi.org/10.1007/s11069-013-0575-4>, 2013.

486 Blair, T.C. & McPherson, J.G.: Processes and forms of alluvial fans. In: PARSONS, A. & ABRAHAMMS, A. (eds)  
487 Geomorphology of Desert Environments, Springer, Dordrecht, The Netherlands, 413–467, doi: [https://doi.org/10.1007/978-1-](https://doi.org/10.1007/978-1-488)  
488 [4020-5719-9\\_14](https://doi.org/10.1007/978-1-4884020-5719-9_14), 2009.

489 Blair, T.C.: Sedimentology of the debris-flow-dominated Warm Spring Canyon alluvial fan, Death Valley, California,  
490 Sedimentology 46 (5), 941–965, doi: <https://doi.org/10.1046/j.1365-3091.1999.00260.x>, 1999.

491 Blikra, L.H., Nemeč, W.: Postglacial colluvium in western Norway: depositional processes, facies and palaeoclimatic record.  
492 Sedimentology 45 (5), 909–960, doi: <https://doi.org/10.1046/j.1365-3091.1998.00200.x>, 1998.

493 Cedillo-Flores, Y., Treiman, A.H., Lasue, J. & Clifford, S.M.: CO<sub>2</sub> gas fluidization in the initiation and formation of Martian  
494 polar gullies, Geophys. Res. Letters, 38, L21202 doi: <https://doi.org/10.1029/2011GL049403>, 2011.

495 Christensen, P.R.: Formation of recent Martian gullies through melting of extensive water-rich snow deposits, Nature, 422,  
496 45–48, doi: <https://doi.org/10.1038/nature01436>, 2003.

497 Conway, S. J., Butcher, F. E., de Haas, T., Deijns, A. A., Grindrod, P. M., & Davis, J. M.: Glacial and gully erosion on Mars:  
498 A terrestrial perspective, Geomorphology, 318, 26-57, doi: <https://doi.org/10.1016/j.geomorph.2018.05.019>, 2018.

499 Conway, S.J. & Balme, M.R.: Decameter thick remnant glacial ice deposits on Mars, Geophys. Res. Letters, 41, 5402–5409,  
500 doi: <https://doi.org/10.1002/2014GL060314>, 2014.

501 Conway, S.J., Balme, M.R., Kreslavsky, M.A., Murray, J.B. & Towner, M.C.: The comparison of topographic long profiles  
502 of gullies on Earth to gullies on Mars: a signal of water on Mars. Icarus, 253, 189–204, doi:  
503 <https://doi.org/10.1016/j.icarus.2015.03.009>, 2015.

504 Conway, S.J., Balme, M.R., Murray, J.B., Towner, M.C., Okubo, C.H. & Grindrod, P.M.: The indication of Martian gully  
505 formation processes by slope–area analysis, In: Balme, M.R., Bargery, A.S., Gallagher, C.J. & Gupta, S. (eds) Martian  
506 Geomorphology, Geological Society, London, Special Publications, 356, 171–201, doi: <https://doi.org/10.1144/SP356.10>,  
507 2011.

508 Conway, S.J., Harrison, T.N., Soare, R.J., Britton, A.W. & Steele, L.J.: New slope-normalized global gully density and  
509 orientation maps for Mars, In: Conway, S.J., Carrivick, J.L., Carling, P.A., De Haas, T. & Harrison, T.N. (eds) Martian Gullies  
510 and their Earth Analogues, Geol. Soc. Lond. Spec. Publ. 467. First published online November 27, 2017, doi:  
511 <https://doi.org/10.1144/SP467.3>, 2017.

512 Costard, F., Forget, F., Mangold, N. & Peulvast, J.P.: Formation of recent Martian debris flows by melting of near-surface  
513 ground ice at high obliquity, Science, 295, 110–113, doi: [10.1126/science.1066](https://doi.org/10.1126/science.1066), 2002.

514 Crosta, G.B., Frattini, P.: Controls on modern alluvial fan processes in the central Alps, northern Italy, *Earth Surf. Proc. Land.*  
515 29 (3), 267–293, doi: <https://doi.org/10.1002/esp.1009>, 2004.

516 de Haas, T., Conway, S.J., Butcher, F.E.G., Levy, J.S., Grindrod, P.M., Balme, M.R., Goudge, T.A.: Time will tell: temporal  
517 evolution of Martian gullies and paleoclimatic implications, *Geol. Soc. Lond. Spec. Publ.* 467, doi:  
518 <https://doi.org/10.1144/SP467.1>, 2019a.

519 de Haas, T., McArdell, B. W., Conway, S. J., McElwaine, J. N., Kleinhans, M. G., Salese, F., & Grindrod, P. M.: Initiation  
520 and flow conditions of contemporary flows in Martian gullies, *J. Geophys. Res.: Planets*, 124(8), 2246-2271, doi:  
521 <https://doi.org/10.1029/2018JE005899>, 2019b.

522 de Haas, T., Hauber, E. & Kleinhans, M.G. 2013. Local late Amazonian boulder breakdown and denudation rate on Mars,  
523 *Geophys. Res. Letters*, 40, 3527–3531, doi: <https://doi.org/10.1002/grl.50726>, 2013.

524 de Haas, T., Ventra, D., Hauber, E., Conway, S.J. & Kleinhans, M.G.: Sedimentological analyses of Martian gullies: the  
525 subsurface as the key to the surface, *Icarus*, 258, 92–108, doi: <https://doi.org/10.1016/j.icarus.2015.06.017>, 2015a.

526 de Haas, T., Kleinhans, M. G., Carbonneau, P. E., Rubensdotter, L., & Hauber, E.: Surface morphology of fans in the high-  
527 Arctic periglacial environment of Svalbard: Controls and processes, *Earth-Science Reviews*, 146, 163-182, doi:  
528 <https://doi.org/10.1016/j.earscirev.2015.04.004>, 2015b.

529 de Scally, F. A., & Owens, I. F.: Morphometric controls and geomorphic responses on fans in the Southern Alps, New Zealand,  
530 *Earth Surface Processes and Landforms: The Journal of the British Geomorphological Research Group*, 29(3), 311-322, doi:  
531 <https://doi.org/10.1002/esp.1022>, 2004.

532 De Scally, F.A., Owens, I.F., Louis, J.: Controls on fan depositional processes in the schist ranges of the Southern Alps, New  
533 Zealand, and implications for debris-flow hazard assessment, *Geomorphology* 122 (1–2), 99–116, doi:  
534 <https://doi.org/10.1016/j.geomorph.2010.06.002>, 2010.

535 Dickson, J.L. & Head, J.W.: The formation and evolution of youthful gullies on Mars: gullies as the latestage phase of Mars  
536 most recent ice age, *Icarus*, 204, 63–86, doi: <https://doi.org/10.1016/j.icarus.2009.06.018>, 2009.

537 Dickson, J.L. et al.: Recent climate cycles on Mars: Stratigraphic relationships between multiple generations of gullies and the  
538 latitude dependent mantle, *Icarus* 252, 83–94, doi: <http://dx.doi.org/10.1016/j.icarus.2014.12.035>, 2015.

539 Dickson, J.L., Head, J.W., Fassett, C.I.: Patterns of accumulation and flow of ice in the mid-latitudes of Mars during the  
540 Amazonian, *Icarus* 219, 723–732, doi: <http://dx.doi.org/10.1016/j.icarus.2012.03.010>, 2012.

541 Dickson, J.L., Head, J.W., Kreslavsky, M.: Martian gullies in the southern midlatitudes of Mars: Evidence for climate-  
542 controlled formation of young fluvial features based upon local and global topography, *Icarus* 188, 315–323, doi:  
543 <https://doi.org/10.1016/j.icarus.2006.11.020>, 2007.

544 Dundas, C. M., McEwen, A. S., Diniega, S., Hansen, C. J., Byrne, S., & McElwaine, J. N.: The formation of gullies on Mars  
545 today, *Geol. Soc. Lond. Spec. Publ.* 467, 67-94, doi: <https://doi.org/10.1144/SP46>, 2019.

546 Dundas, C.M., Diniega, S., Hansen, C.J., Byrne, S., McEwen, A.S.: Seasonal activity and morphological changes in martian  
547 gullies, *Icarus* 220:124–143, doi: <https://doi.org/10.1016/j.icarus.2012.04.005>, 2012.

548 Dundas, C.M., Diniega, S., McEwen, A.S.: Long-term monitoring of Martian gully formation and evolution with  
549 MRO/HiRISE, *Icarus* 251:244–263, doi: <https://doi.org/10.1016/j.icarus.2014.05.013>, 2015.

550 Hargitai, H. (2014). Viscous Flow Features (Mars). In: *Encyclopedia of Planetary Landforms*. Springer, New York, NY.  
551 [https://doi.org/10.1007/978-1-4614-9213-9\\_596-1](https://doi.org/10.1007/978-1-4614-9213-9_596-1)

552 Harrison, T.N., Osinski, G.R., Tornabene, L.L., Jones, E.: Global documentation of gullies with the Mars reconnaissance  
553 orbiter context camera and implications for their formation, *Icarus* 252:236–254, doi:  
554 <https://doi.org/10.1016/j.icarus.2015.01.022>, 2015.

555 Hartley, A.J., Mather, A.E., Jolley, E., Turner, P.: Climatic controls on alluvial-fan activity, Coastal Cordillera, northern Chile.  
556 In: Harvey, A.M., Mather, A.E., Stokes, M. (Eds.), *Alluvial Fans: Geomorphology, Sedimentology, Dynamics*. *Geol. Soc.*  
557 *Lond. Spec. Publ.* 251, 95-115, doi: <https://doi.org/10.1144/GSL.SP.2005.251.01.>, 2005.

558 Head, J.W., Marchant, D.R., Dickson, J.L., Kress, A.M., Baker, D.M.: Northern midlatitude glaciation in the Late Amazonian  
559 period of Mars: criteria for the recognition of debris-covered glacier and valley glacier landsystem deposits, *Earth Planet. Sci.*  
560 *Lett.* 294:306–320, doi: <https://doi.org/10.1016/j.epsl.2009.06.041>, 2010.

561 HELDMANN, J.L. & MELLON, M.T.: Observations of Martian gullies and constraints on potential formation mechanisms,  
562 *Icarus*, 168, 285–304, doi: <https://doi.org/10.1016/j.icarus.2003.11.024>, 2004.

563 Heldmann, J.L. et al.: Formation of martian gullies by the action of liquid water flowing under current martian environmental  
564 conditions, *J. Geophys. Res. Planets* 110, doi: <http://dx.doi.org/10.1029/2004JE002261>, 2005.

565 Hobbs, S.W., Paull, D.J., Clark, J.D.A.: A comparison of semiarid and subhumid terrestrial gullies with gullies on Mars:  
566 Implications for martian gully erosion, *Geomorphology* 204, 344–365, doi: <http://dx.doi.org/10.1016/j.geomorph.2013.08.018>,  
567 2014.

568 Hobbs, S.W., Paull, D.J. and Clarke, J.D.A.: Analysis of regional gullies within Noachis Terra, Mars: A complex relationship  
569 between slope, surface material and aspect, *Icarus*, 250, 308-331, doi: <https://doi.org/10.1016/j.icarus.2014.12.011>, 2015.

570 Hubbard, B., Milliken, R.E., Kargel, J.S., Limaye, A. & Souness, C.: Geomorphological characterisation and interpretation of  
571 a mid-latitude glacier-like form: Hellas Planitia, Mars, *Icarus*, 211, 330–346, doi: <https://doi.org/10.1016/j.icarus.2010.10.021>,  
572 2011.

573 Ilinca, V.: Using morphometrics to distinguish between debris flow, debris flood and flood (Southern Carpathians, Romania),  
574 *Catena*, 197, 104982, doi: <https://doi.org/10.1016/j.catena.2020.104982>, 2021.

575 Jackson LE, Kostaschuk RA, MacDonald GM: Identification of debris flow hazard on alluvial fans in the Canadian Rocky  
576 Mountains, In: Costa JE, Wicczorek GF (eds) Debris flows/avalanches: process, recognition, and mitigation. *Rev Eng Geol*  
577 vol. VII. Geol. Soc. Am, doi: <https://doi.org/10.1130/REG7-p115>, 1987.

578 Johnsson, A. et al.: Evidence for very recent melt-water and debris flow activity in gullies in a young mid-latitude crater on  
579 Mars, *Icarus* 235, 37–54, doi: <http://dx.doi.org/10.1016/j.icarus.2014.03.005>, 2014.

580 Kirk, R.L., Howington-Kraus, E., Rosiek, M.R., Anderson, J.A., Archinal, B.A., Becker, K.J., Cook, D.A., Galuszka, D.M.,  
581 Geessler, P.E., Hare, T.M., Holmberg, I.M., Keszthelyi, L.P., Redding, B.L., Delamere, W.A., Gallagher, D., Chapel, J.D.,  
582 Eliason, E.M., King, R., McEwen, A.S.: Ultrahigh resolution topographic mapping of Mars with MRO HiRISE stereo images:  
583 meter-scale slopes of candidate Phoenix landing sites, *J. Geophys. Res. Planets* 113, doi:  
584 <https://doi.org/10.1029/2007JE003000>, 2008.

585 Kostaschuk, R.A., Macdonald, G.M., Putnam, P.E.: Depositional process and alluvial fan-drainage basin morphometric  
586 relationships near Banff, Alberta, Canada, *Earth Surf. Proc. Land.* 11 (5), 471–484, doi:  
587 <https://doi.org/10.1002/esp.3290110502>, 1986.

588 Kreslavsky, M.A.: Slope steepness of channels and aprons: Implications for origin of martian gullies. Workshop Martian  
589 Gullies, Workshop on Martian Gullies 2008. Abs.#1301, 2008.

590 Kreslavsky, M.A., Head, J.W.: Mars: nature and evolution of young latitudedependent water-ice-rich mantle, *Geophys. Res.*  
591 *Lett.* 29, doi: <https://doi.org/10.1029/2002GL015392>, 2002.

592 Langbein, W. B.: Profiles of rivers of uniform discharge, *U.S. Geol. Surv. Prof. Pap.*, 501-B, 119– 122, doi:  
593 <https://doi.org/10.1086/627653>, 1964.

594 Lanza, N. L., Meyer, G. A., Okubo, C. H., Newsom, H. E., & Wiens, R. C.: Evidence for debris flow gully formation initiated  
595 by shallow subsurface water on Mars, *Icarus*, 205(1), 103-112, doi: <https://doi.org/10.1016/j.icarus.2009.04.014>, 2010.

596 Levy, J.S. et al.: Identification of gully debris flow deposits in Protonilus Mensae, Mars: Characterization of a water-bearing,  
597 energetic gully-forming process, *Earth Planet. Sci. Lett. Mars Express after 6 Years in Orbit: Mars Geology from Three-*  
598 *Dimensional Mapping by the High Resolution Stereo Camera (HRSC) Experiment* 294, 368–377, doi:  
599 <https://doi.org/10.1016/j.epsl.2009.08.002>, 2010b.

600 Levy, J.S., Head, J., Marchant, D.: Thermal contraction crack polygons on Mars: classification, distribution, and climate  
601 implications from HiRISE observations, *J. Geophys. Res. Planets* 114, 01007, doi: <https://doi.org/10.1029/2008JE003273>,  
602 2009a.

603 Levy, J. S., Head, J. W., Marchant, D. R., Dickson, J. L., & Morgan, G. A.: Geologically recent gully–polygon relationships  
604 on Mars: Insights from the Antarctic Dry Valleys on the roles of permafrost, microclimates, and water sources for surface  
605 flow, *Icarus*, 201(1), 113-126, doi: <https://doi.org/10.1016/j.icarus.2008.12.043>, 2009b.

606 Levy, J.S., Head, J.W., Marchant, D.R.: Gullies, polygons and mantles in Martian permafrost environments: cold desert  
607 landforms and sedimentary processes during recent Martian geological history, *Geol. Soc. Lond. Spec. Publ.* 354, 167–182,  
608 doi: <https://doi.org/10.1144/SP354.10>, 2011.

609 Malin, M.C., Edgett, K.S.: Evidence for recent groundwater seepage and surface runoff on Mars. *Science* 288:2330–2335, doi:  
610 <https://doi.org/10.1126/science.288.5475.2330>, 2000.

611 McEwen, A.S., Eliason, E.M. et al.: Mars reconnaissance orbiter’s High Resolution Imaging Science Experiment (HiRISE), *J.*  
612 *Geophys. Res.: Planets*, 112, E05S02, doi: <https://doi.org/10.1029/2005JE002605>, 2007.

613 McLachlan, G. J.: Discriminant analysis and statistical pattern recognition, John Wiley & Sons, 2005.

614 Melton, M.A.: An analysis of the relation among elements of climate, surface properties and geomorphology, Office of Nav.  
615 Res. Dept. Geol. Columbia Univ, NY. Tech. Rep. 11, 1975.

616 Milliken, R.E., Mustard, J.F., Goldsby, D.L.: Viscous flow features on the surface of Mars: observations from high-resolution  
617 Mars Orbiter Camera (MOC) images, *J. Geophys. Res.* 108, doi: <https://doi.org/10.1029/2002JE002005>, 2003.

618 Mustard, J.F., Cooper, C.D., Rifkin, M.K.: Evidence for recent climate change on Mars from the identification of youthful  
619 near-surface ground ice, *Nature* 412:411–414, doi: <https://doi.org/10.1038/35086515>, 2001.

620 Phillips, J.D., Lutz, J.D.: Profile convexities in bedrock and alluvial streams, *Geomorphology* 102, 554–566, doi:  
621 <https://doi.org/10.1016/j.geomorph.2008.05.042>, 2008.

622 Pilonget, C. & Forget: Formation of gullies on Mars by debris flows triggered by CO<sub>2</sub> sublimation, *Nature Geoscience*, 9, 65–  
623 69, doi: <https://doi.org/10.1038/ngeo2619>, 2016.

624 Plaut, Jeffrey J., Ali Safaeinili, John W. Holt, Roger J. Phillips, James W. Head III, Roberto Seu, Nathaniel E. Putzig, and  
625 Alessandro Frigeri: Radar evidence for ice in lobate debris aprons in the mid-northern latitudes of Mars, *Geophysical research*  
626 *letters* 36, no. 2, doi: <https://doi.org/10.1029/2008GL036379>.

627 Reiss, D. et al.: Absolute dune ages and implications for the time of formation of gullies in Nirgal Vallis, Mars. *J. Geophys.*  
628 *Res.-Planets* 109, doi: <http://dx.doi.org/10.1029/2004JE002251>, 2004.

629 Reiss, D., Hauber, E. et al.: Terrestrial gullies and debris-flow tracks on Svalbard as planetary analogs for Mars, In: Garry,  
630 W.B. & Bleacher, J.E. (eds) *Analogues for Planetary Exploration*, Geol. Soc. Am. Spec. Papers 483, 165–175, doi:  
631 [https://doi.org/10.1130/2011.2483\(11\)](https://doi.org/10.1130/2011.2483(11)), 2011.

632 Rodine, J.D., Johnson, A.M.: The ability of debris, heavily freighted with coarse clastic materials, to flow on gentle slopes,  
633 *Sedimentology* 23, 213–234, doi: <https://doi.org/10.1111/j.1365-3091.1976.tb00047.x>, 1976.

634 Ryder, J.: Some aspects of the morphometry of paraglacial alluvial fans in South-central British Columbia, *Canadian Journal*  
635 *of Earth Sciences* 8: 1252-1264, doi: <https://doi.org/10.1139/e71-11>, 1971.

636 Schon, S.C., Head, J.W., Fassett, C.I.: Unique chronostratigraphic marker in depositional fan stratigraphy on Mars: Evidence  
637 for ca. 1.25 Ma gully activity and surficial meltwater origin, *Geology* 37, 207–210, doi: <http://dx.doi.org/10.1130/g25398a.1>,  
638 2009.

639 Siewert, M. B., Krautblatter, M., Christiansen, H. H., & Eckerstorfer, M.: Arctic rockwall retreat rates estimated using  
640 laboratory-calibrated ERT measurements of talus cones in Longyeardalen, Svalbard, *Earth Surface Processes and Landforms*,  
641 37(14), 1542-1555, doi: <https://doi.org/10.1002/esp.3297>, 2012.

642 Sinha, R. K., Ray, D., De Haas, T., & Conway, S. J.: Global documentation of overlapping lobate deposits in Martian gullies.  
643 *Icarus*, 352, 113979, doi: <https://doi.org/10.1016/j.icarus.2020.113979>, 2020.

644 Sinha, R. K., Vijayan, S., Shukla, A. D., Das, P., & Bhattacharya, F.: Gullies and debris-flows in Ladakh Himalaya, India: a  
645 potential Martian analogue, *Geol. Soc. Lond. Spec. Publ.* 467, 315-342, doi: <https://doi.org/10.1144/SP46>, 2019.

646 Sinha, R.K., Vijayan, S.: Geomorphic investigation of craters in Alba Mons, Mars: implications for Late Amazonian glacial  
647 activity in the region, *Planet. Space Sci.* 144:32–48, doi: <https://doi.org/10.1016/j.pss.2017.05.014>, 2017.

648 Souness, C., & Hubbard, B.: Mid-latitude glaciation on Mars, *Progress in Physical Geography*, 36(2), 238-261, doi:  
649 <https://doi.org/10.1177/030913331243>, 2012.

650 Souness, C., Hubbard, B., Milliken, R. E., & Quincey, D.: An inventory and population-scale analysis of martian glacier-like  
651 forms, *Icarus*, 217(1), 243-255, doi: <https://doi.org/10.1016/j.icarus.2011.10.020>, 2012.

652 Stock, J.D., Dietrich, W.E.: Erosion of steepland valleys by debris flow, *Geol. Soc. Am. Bull.* 118 (9/10), 1125–1148.  
653 doi:10.1130/B25902.1, 2006.

654 Stolle, A., Langer, M., Blöthe, J. H., & Korup, O.: On predicting debris flows in arid mountain belts, *Global and Planetary*  
655 *Change*, 126, 1-13, doi: <https://doi.org/10.1016/j.gloplacha.2014.12.005>, 2015.

656 Welsh, A., Davies, T.: Identification of alluvial fans susceptible to debris-flow hazards. *Landslides* 8 (2), 183–194, doi:  
657 <https://doi.org/10.1007/s10346-010-0238-4>, 2011.

658 Wilford, D. J., Sakals, M. E., Innes, J. L., Sidle, R. C., & Bergerud, W. A.: Recognition of debris flow, debris flood and flood  
659 hazard through watershed morphometrics, *Landslides*, 1(1), 61-66, doi: <https://doi.org/10.1007/s10346-003-0002-0>, 2004.

660 Yue, Z., Hu, W., Liu, B., Liu, Y., Sun, X., Zhao, Q. and Di, K.: Quantitative analysis of the morphology of martian gullies and  
661 insights into their formation, *Icarus*, 243, pp.208-221, doi: <https://doi.org/10.1016/j.icarus.2014.08.028>, 2014.

662